JOURNAL OF MATERIALS SCIENCE 29 (1994) 2152–2158

# Influence of copper- and iron-doping on cubic yttria-stabilized zirconia

M. HARTMANOVA
*Institute of Physics, Slovak Academy of Sciences, 84228 Bratislava, Slovakia*

F. W. POULSEN*
*Laboratories of Industrial Electrochemistry, NTH, 7034 Trondheim, Norway*

F. HANIC, K. PUTYERA, D. TUNEGA
*Institute of Inorganic Chemistry, Slovak Academy of Sciences, 84236 Bratislava, Slovakia*

A. A. URUSOVSKAYA, T. V. ORESHNIKOVA
*Institute of Crystallography, Russian Academy of Sciences, 117333 Moscow, Russia*

Cubic yttria-stabilized zirconias (YSZs) (15 mol % $Y_2O_3$) doped with 2 wt % CuO and 0.3 wt % $Fe_2O_3$, respectively, have been compared with undoped YSZ. The lattice constants were found to increase in the sequence: $a_{YSZ} < a_{YSZ/Fe} < a_{YSZ/Cu}$. Vickers microhardness of polycrystalline YSZ/Fe exceeds that of polycrystalline YSZ/Cu, whereas the hardness of the single crystalline materials YSZ/Fe and YSZ/Cu are nearly identical and consistently lower than the polycrystalline values. Raman and infrared spectra reveal a breakdown of the selection rules, i.e. these techniques probe the local, non-cubic arrangement of oxygen vacancies. The findings are discussed in terms of a substitutional versus an interstitial-doping model.

## 1. Introduction

Cubic stabilized zirconia containing various transition metal oxides have been studied in several laboratories [1–13]. There is relatively little known, however, concerning the introduction of copper into zirconia, e.g. [10, 13–15]. It was the purpose of the present investigation to study copper- and iron-doping of YSZ. Precise lattice constant determinations, ionic conductivity data, Raman and infrared spectra and microhardness data are presented for copper- and iron-doped YSZ. Comparisons are made with single-crystal data as well as data for "undoped" YSZ of the same yttria content. The dopant level of copper and iron used in this work (0.3–2 wt %) is on the same level as chromophore additions in zirconia-based synthetic jewels. Also, the addition of grain-growth inhibitors (alumina) or grain-boundary clean-up agents (i.e. SrO) lies in this range [13].

## 2. Experimental procedure

### 2.1. Preparation of samples

Samples of YSZ ceramics doped with 2 wt % CuO and 0.3 wt % $Fe_2O_3$ were prepared from powder forms of the corresponding oxides. The mixtures were homogenized by ball milling for 2 h and then heated to 1640 K. The calcined products were reground by ball milling for 24 h, then pressed into disc form at 100 MPa. The discs were sintered in air with a 1 h holding time at 1950 K.

The single crystals were made by direct inductive melting of the oxides using the "cold crucible" technique [16].

The experimental densities, $d_0$, of the samples were determined in a modified Amsler apparatus constructed on the principle of uplift of samples immersed in mercury. The mercury does not enter the open pores owing to a capillary depression. The densities listed in Table I represent arithmetical means from five parallel measurements. The porosity (open and closed), $p$, was calculated from the theoretical X-ray density (assuming an interstitial doping mechanism).

The polished discs were examined in an electron probe microanalyser, type Jeol JXA-840 A, in order to determine the elemental distribution of zirconium, yttrium, copper and iron.

### 2.2. Crystal structure and microstructure

The lattice parameters were evaluated from indexed powder diffraction data on a Philips PW 1050 diffractometer using Cu$K_\alpha$ radiation. α-alumina (1:1) was used as an internal standard. The quantitative analysis of the microstructure was done on an SEM Tesla BS 300 microscope at an acceleration voltage of 25 keV. The intercept length method was used for quantitative measurements [17].

* *Permanent address*: RISØ National Laboratory, DK-4000 Roskilde, Denmark



0022–2461 

TABLE I Crystal data for pure and iron- and copper-doped YSZ. $a$, cubic lattice parameter; $V$, unit cell volume; molar mass ($Z = 4$) calculated for the interstitial model, cf. Section 4; theoretical density from X-ray data $D_X$; $D_o$, observed density for polycrystalline material; $p$ porosity.

| Sample | $a$ (nm) | $V$ ($10^{-3}$ nm$^3$) | $M_w$ (g mol$^{-1}$) | $D_X$ (g cm$^{-3}$) | $D_o$ (g cm$^{-3}$) | $p$ (%) |
|---|---|---|---|---|---|---|
| Pure YSZ 15 mol % $Y_2O_3$ | 0.515 72(3) | 137.16 | 482.104 | 5.835 | 5.521 | 5.4 |
| + 0.3 wt % $Fe_2O_3$ | 0.516 32(15) | 137.64 | 483.55 | 5.833 | 5.240 | 10.2 |
| + 2.0 wt % CuO | 0.516 79(3) | 138.02 | 491.746 | 5.915 | 5.131 | 13.3 |

## 2.3. Ionic conductivity

The platinum paste electrodes were applied to the entire circular faces of the discs. The samples were heated to 900 °C for 3 h in order to remove the binders. The samples were placed between platinum-foil current collectors. The temperature was measured with a Ni/CrNi thermocouple, uncertainty 1 °C below 500 °C, and 3 °C above. The impedance was determined in air, at 40–50 different frequencies between 0.1 Hz and 1 MHz by a solartron 1174 FRA. The detailed method of analysing the admittance data is described elsewhere [18].

## 2.4. Microhardness

The microhardness was determined by means of indentation of a Vickers pyramid. The indentation was performed on a module of the metallographic microscope Neophot-21. The load, $P$, on the indentor was varied from 0.05–1 N. This permitted evaluation of the microhardness, $H$, at different depths, $h$, from the sample surface (0.2–0.4 μm). The investigation was made on the plane perpendicular to the crystal-growth axis.

## 2.5. Raman and infrared spectra at room temperature

The infrared reflectance measurements with the near normal incidence angle were carried out on a Perkin–Elmer 9836 Spectrophotometer in the range 180–900 cm$^{-1}$ and were compared with the front-aluminized mirror.

The unpolarized Raman spectra were measured on the (unoriented) samples. The 488 nm line of an $Ar^+$ laser was used as the excitation; the power of the beam at the sample was 350 mW. The scattered light was analysed by a Jeol JRS S-1 Spectrometer equipped with a double grating monochromator. All measurements were made using a right-angle geometry.

# 3. Results

## 3.1. Lattice parameter and formation of solid solution

The following formula was used for the evaluation of the lattice parameter, $a$, of the cubic structure from the known diffraction angles, θ, and the indices $h$, $k$, $l$ of the selected pairs of diffraction lines $i$, $j$

$$a = \frac{\lambda}{2\sin\Delta_{ij}}(h_i^2 + k_i^2 + l_i^2)^{1/2}\cos\theta_i - (h_j^2 + k_j^2 + l_j^2)^{1/2}\cos\theta_j \quad (1)$$

where $\Delta_{ij} = \theta_i - \theta_j$. This method of evaluation, based on differences of the $\Delta_{ij}$ values minimizes the errors caused by imperfect centring of the samples (zero-point error) or by absorption of X-ray radiation. The lattice parameters (upper curves in Fig. 1a and b) calculated in this way prove to be independent of the diffraction angle. The selective standard deviation, $s_a$, of the value $a$, was calculated according to the relation

$$s_a = (s_a^2)^{1/2} \quad (2)$$

where

$$s_a^2 = 1/(n-1)\left[\sum a_i^2 - 1/n(\sum a_i)^2\right] \quad (3)$$

and the summations run over $n$ number of data.

The crystallographic data summarized in Table I show that CuO and $Fe_2O_3$ dissolve in the cubic fluorite structure. No additional phases were identified in the powder diffraction patterns. The lattice parameters, $a$, of the doped samples increase (compared to YSZ) with the amount of oxide added.

The average grain size of undoped YSZ was found to be 7.7 μm. The CuO-doped YSZ had a mean grain size of 13.3 μm, while that of $Fe_2O_3$-doped YSZ was 12.5 μm. The investigated ceramic samples have a log-normal grain-size distribution. No influence of the kind of additive was thus observed. The quite large grain sizes were a result of the high sintering temperature (1950 K). The elemental distribution investigated by means of the microprobe confirmed the conclusion of the X-ray study regarding the absence of any secondary phase at the grain boundaries. According to the micrographs, both additives are homogeneously distributed.

## 3.2. Ionic conductivity

The a.c.-admittance technique has been demonstrated to be a powerful tool for characterization of solid electrolytes, such as YSZ [18, 19]. The bulk, grain-boundary, and electrode processes can often be separated in a single experiment. A typical example of the admittance data obtained in the presented study is shown in Fig. 2a. Each data set is characterized by two semicircles, which then allow determination of three resistances and two capacitive elements. The bulk and grain-boundary conductivities could be resolved in the range 250–916 °C. In order to obtain reasonable fit to the low-frequency electrode part of the response, we invoked a CPA element (instead of a simple capacitor) [18] in parallel with the electrode resistance, see Fig. 2. An example of fitted values to two data sets obtained at approximately the same temperature for the YSZ/Cu and YSZ/Fe samples is given in Table II. As can be

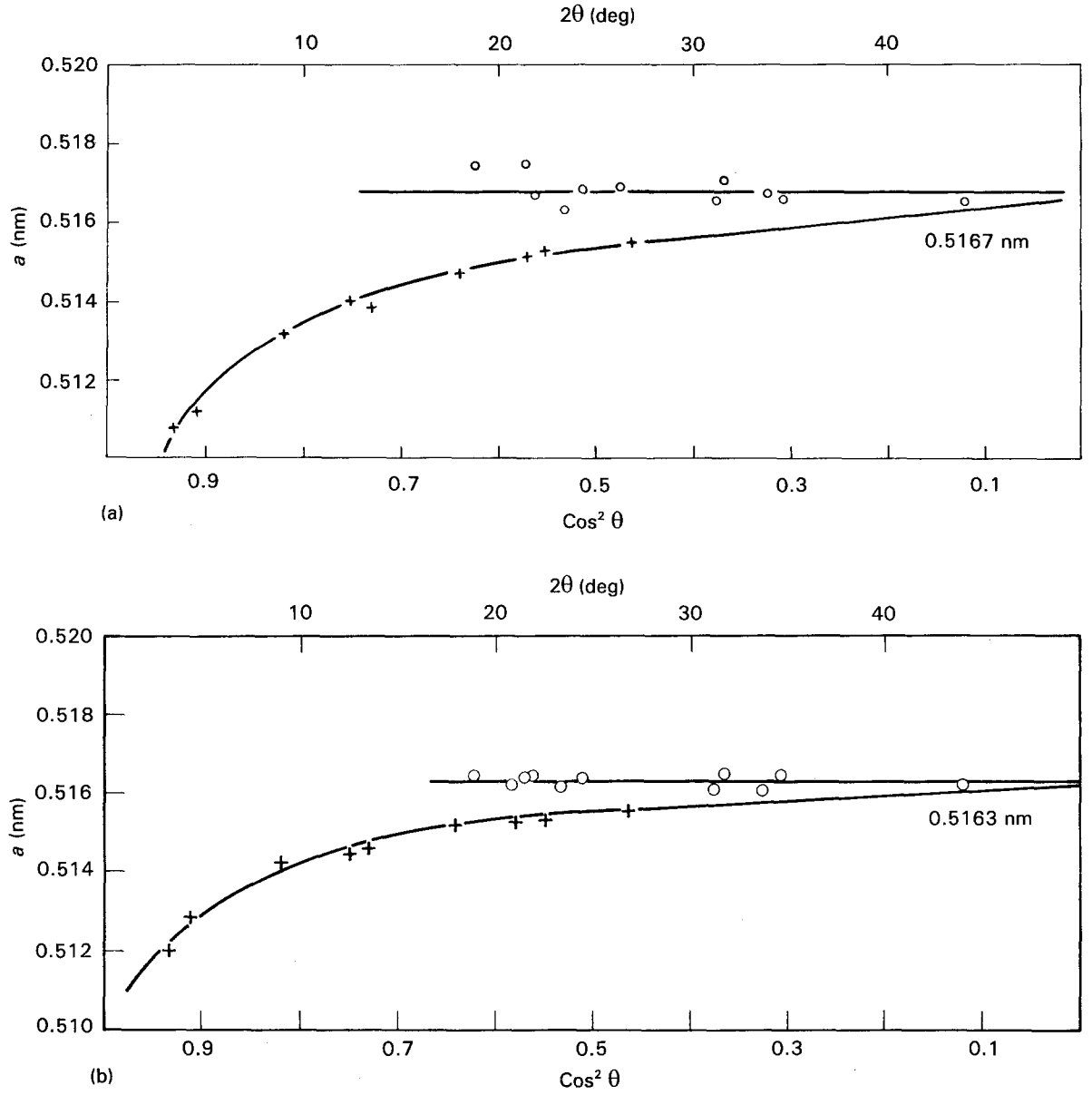


*Figure 1* Comparison of lattice parameter, $a$, calculated from Equation 1 (upper curves) with the uncorrected $a$-value, for (a) YSZ + CuO, (b) YSZ + $Fe_2O_3$.

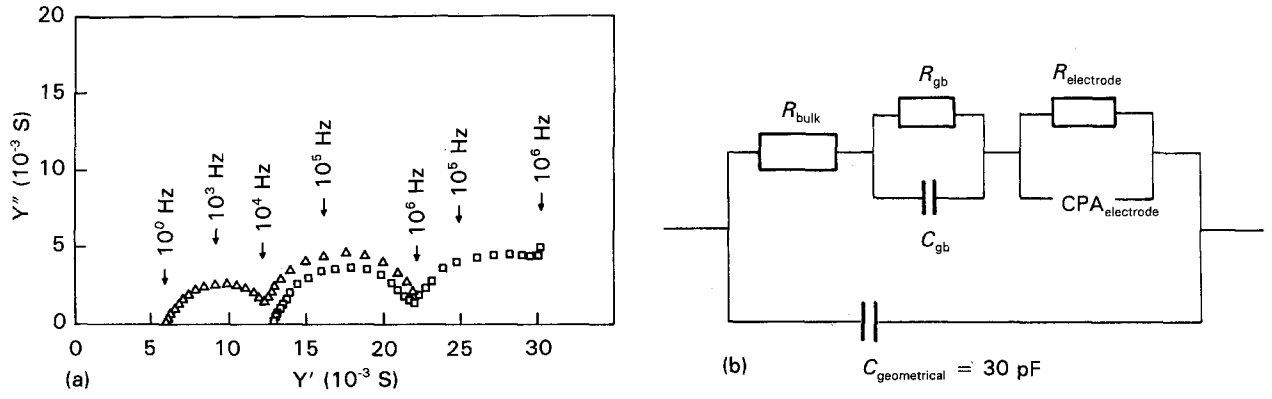


*Figure 2* (a) Admittance diagrams for (□) iron- and △ copper-doped polycrystalline YSZ in symmetrical cells of the type air|Pt|YSZ|Pt|air. (□) 759.9 °C, $L/A = 0.1952\ cm^{-1}$. (△) $T = 763.4$ °C, $L/A = 0.1402\ cm^{-1}$. (b) Appropriate equivalent circuit for data fitting.

seen, the iron-doped sample has a better ionic conductivity (and also electrode performance) than the copper-doped one. The activation energies and pre-exponential parameters according to the general expression $\sigma = \sigma_0 \exp(-\Delta E_a/kT)$ are given in Table III. In the investigated temperature range the conductivity is entirely ionic for both samples studied in air. This is in a good agreement with transport

TABLE II Fitted circuit parameters to the $\{[R(RC)(RQ)]C\}$ model

| | Sample | |
|---|---|---|
| | YSZ + $Fe_2O_3$ | YSZ + CuO |
| Temp. (°C) | 759.9 | 763.4 |
| $R_{bulk}$ (Ω) | 31.2 | 44.9 |
| $R_{gb}$ (Ω) | 14.6 | 32.4 |
| $C_{gb}$ (nF) | 73.1 | 62.9 |
| $R_{electrode}$ (Ω) | 30.8 | 92.7 |
| $CPA_{electrode}$ ("Ω") | $6.15 \times 10^4$ | $4.4 \times 10^4$ |
| Exponent in CPA | − 0.9805 | − 0.7840 |
| Length/area ($cm^{-1}$) | 0.1952 | 0.1402 |

TABLE III Constants in Arrhenius equation for the investigated YSZ materials

| | | YSZ + Fe | YSZ + CuO | YSZ (reference) |
|---|---|---|---|---|
| Bulk | $\Delta E$ (eV) | 1.24 ± 0.018 | 1.208 ± 0.038 | |
| | $\log_{10}(\sigma_o)$ ($S\,cm^{-1}$) | 3.691 | 3.513 | |
| Grain Boundary | $\Delta E$ (eV) | 1.329 ± 0.065 | 1.332 ± 0.037 | |
| | $\log_{10}(\sigma_o)$ ($S\,cm^{-1}$) | 4.569 | 4.232 | |
| Total | $\Delta E$ (eV) | 1.267 ± 0.012 | 1.222 ± 0.035 | 1.252 ± 0.03 |
| | $\log_{10}(\sigma_o)$ ($S\,cm^{-1}$) | 3.674 | 3.326 | 3.349 |
| Number of temperatures | | 19 | 22 | – |

number measurements carried out under the same conditions [2]. In order to compare the effects of dopant addition on the electrical conductivity of the present YSZ (highly yttria-doped), we have included data for pure YSZ in Table III and Fig. 3.

The ionic conductivity of YSZ as a function of yttria content is assumed to attain its maximum value around 8 mol % $Y_2O_3$. The creation of more oxygen vacancies by addition of more yttria or other lower valent oxides beyond the 8 mol% level will, therefore, be expected to lead to a decrease in the oxygen ion conductivity. This is a combined effect of an increase of the activation energy and increased association of vacancies with dopant ions at higher defect concentrations. The pure YSZ data in Fig. 3 refer to a smaller grain size (7.7 μm) than the doped samples – the somewhat higher grain-boundary contribution to the resistance therefore gives a slightly smaller conductivity than for the doped YSZ. By and large, however, we observe that the conductivity decreases with increasing amount of added oxide. It has been suggested that if the added oxide is uniformly distributed throughout the sample volume, the relative change in bulk and grain-boundary conductivity should be the same [20]. Owing to the use of only one concentration for each type of dopant we are not able to test this hypothesis.

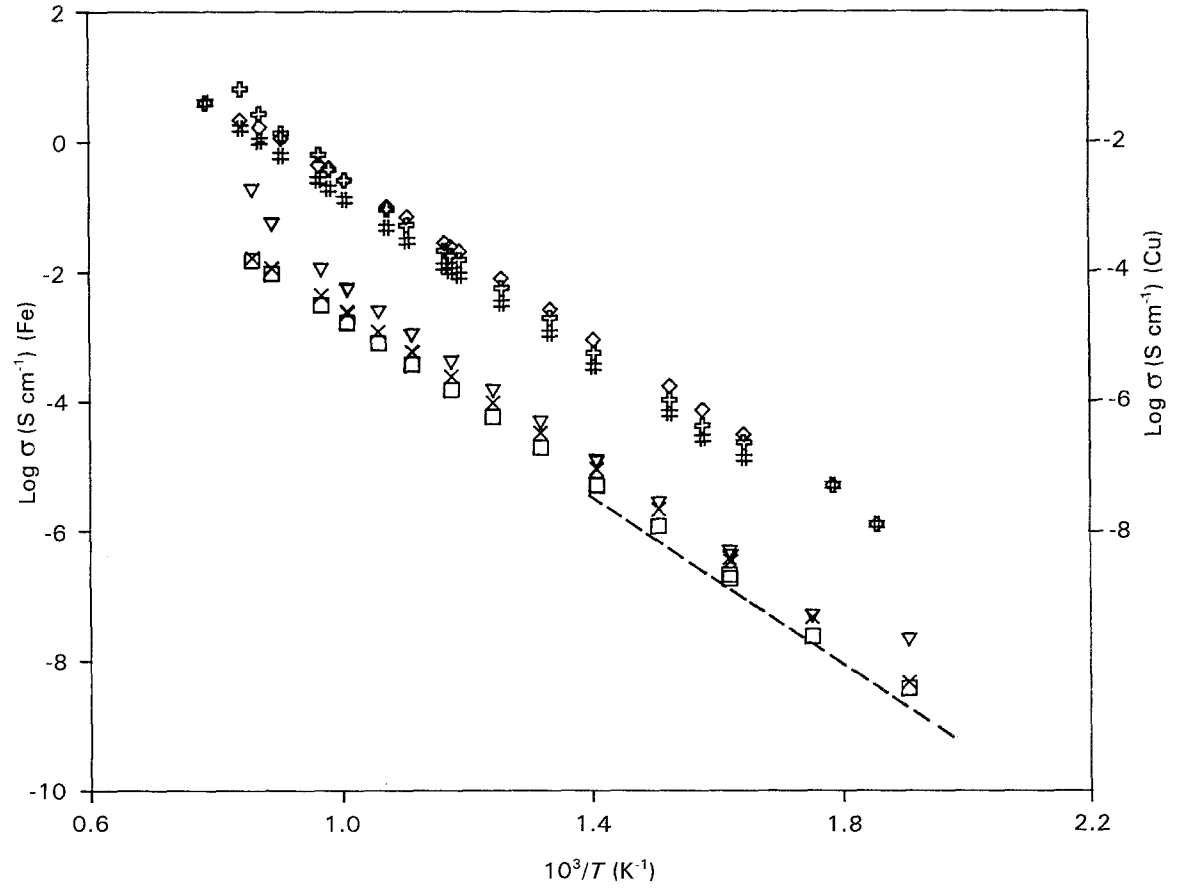


*Figure 3* Arrhenius plot. (– – –) Conductivity level for pure 15 mol % YSZ (reference). Cu: (#) total, (◇) bulk, (⊕) grain boundary. Fe: (□) total, (×) bulk, (▽) grain boundary.

If all the added oxide was forming a grain-boundary phase, the impact on the conductivity would be usually negative. An increase of the conductivity due to cleaning of grain boundaries by addition of a non-soluble oxide (e.g. SrO) has also been observed [13]. The grain-boundary capacities for YSZ/Fe and YSZ/Cu were nearly temperature independent. At approximately 760 °C they amount to 73–87 nF and 62–65 nF, respectively. These values scale with the inverse of the thickness of the two samples, as expected for ideal capacitors (the samples had the same area and grain size). The activation energy for grain-boundary conduction is higher than for bulk conduction. This is a general trend also observed for YSZs with lower yttria-dopant levels. Our data for YSZ/Fe agree well with the data of Matsui and Takigawa [5]. The ratio $R_{gb}/R_b$ for YSZ/Fe varies from 1 at low temperature to $\sim 0.1$ at high temperature. The corresponding values for the YSZ/Cu sample span the range from 1.7 at low temperature to 0.33 at high temperature.

## 3.3. Microhardness of single crystals and ceramics of the same composition

It is well known that the Vickers microhardness is load-dependent at low indentation loads, the hardness decreasing with increasing indentation to a constant level at high loads. The hardness was calculated using the standard equation for the Vickers pyramid geometry

$$H = 1.8554P/d^2 \quad (4)$$

where $P$ is the indentation load and $d$ is the indent diagonal.

Only a limited number of indentation studies has been reported on cubic zirconia. The anisotropy in the microhardness of single crystals has been determined by several investigators [21, 22]. The change of the microhardness with load for the present samples is shown in Fig. 4a and b, in which polycrystalline samples are compared with single crystals with the same dopant. The microhardness of the single crystals is nearly the same near the surface ($P = 0.05$ N) and in the bulk ($P = 1$ N), independent of whether they are copper- or iron-doped. On the other hand, the microhardness of the ceramics varies much more with the load (see Fig. 4a and b, curves 2). The YSZ/Fe is approximately 1.3 harder than their corresponding single-crystal materials of the same composition. The reproducibility of indent dimension in different regions of the samples was good, the scatter in $H$ values being no more than 5%–6%. The indentation is within a single grain at loads lower than 0.5 N. At higher loads, two to four grains are involved in the indent.

In conclusion, the ceramics were, as expected, harder than the single crystals of the same composition – the surface hardness was up to three to four times higher for the ceramics than for the single crystals; both additives cause hardening compared to pure YSZ [23]. The iron-doping gives harder material than the copper-doping, though iron was present in a smaller amount.

## 3.4. Raman and infrared spectra

Raman and infrared spectroscopy are often used in order to confirm the structural modifications, phase transitions and regions of mixed structures [24–33]. The crystal structure of YSZ is of the fluorite type ($Z = 4$). The zirconium ion "sublattice" has a perfect fcc structure, where $Zr^{4+}$ ions are randomly substituted by $Y^{3+}$ ions. The oxygen ion sublattice is primitive cubic. A certain number of oxygen sites are vacant in order to maintain electroneutrality. This anion disorder means that the individual unit cells of YSZ do not have any translation symmetry. This destroys the wave vector $\boldsymbol{k} = 0$ selection rule for Raman scattering (and similarly for infrared absorption) in such a way that the Raman spectra reflect the frequency distribution of the density of the state of phonons [29, 32, 34, 35]. The irreducible representations of the Raman modes have previously been determined by polarization measurements and factor group analysis of disordered YSZs [26, 27, 30, 33, 36]. Only one, triply degenerated sharp band of $F_{2g}$ symmetry is expected for an ideal fcc structure, but for the disordered structures, several additional broader Raman bands were observed. Furthermore, the $F_{2g}$ mode is broadened (up to 200 $cm^{-1}$ half-width), compared to what is observed for perfect fcc structures. Ishigame and Yoshida [30] have shown that the additional bands and their broadening, have their origin in a defect-induced first-order Raman effect. They also performed the lattice dynamics calculations in the rigid-ion approximation, where they took into account the defect space consisting of the vacancy and the nearest six (displaced) oxygen ions, but neglecting the surrounding four metal ions. This calculation showed a good agreement between the calculated frequency distribution and the measured Raman spectra. The conclusion of

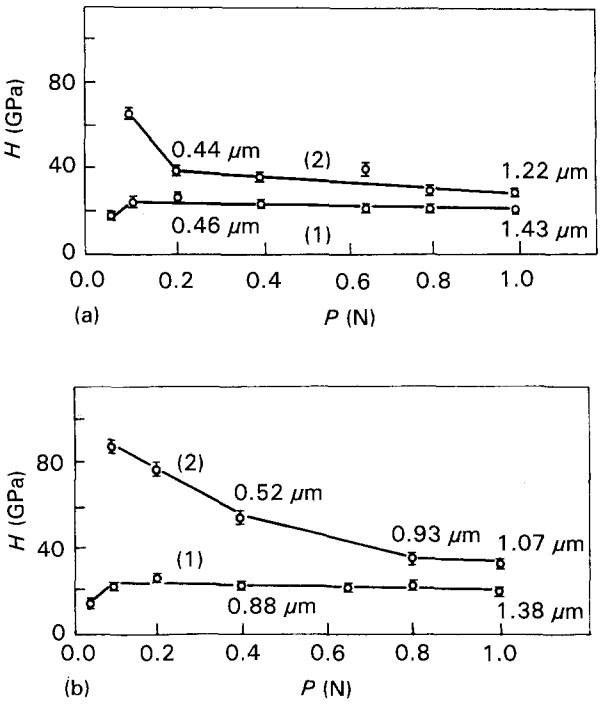


*Figure 4* Change in microhardness with increasing load on the indentor, for (a) YSZ + CuO, (b) YSZ + $Fe_2O_3$. Curves 1, single-crystalline YSZ; curves 2, polycrystalline ceramics.

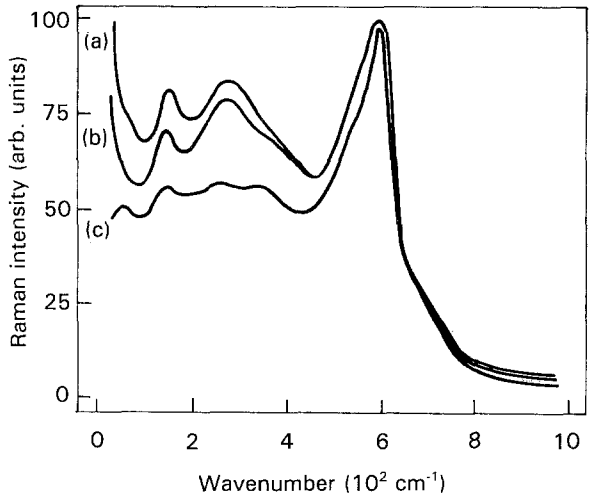


*Figure 5* Raman spectra of (a) single crystalline YSZ, (b) YSZ + CuO and (c) YSZ + $Fe_2O_3$.

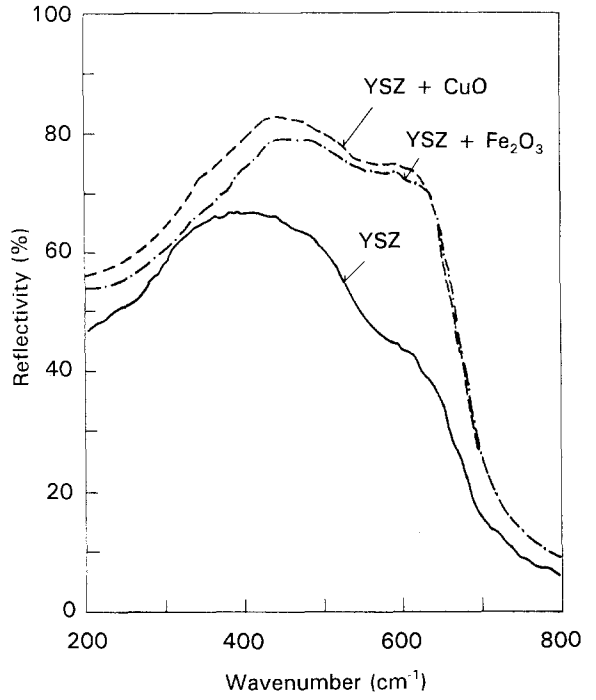


*Figure 6* Infrared reflectance spectra of (a) single-crystalline YSZ, (b) YSZ + CuO and (c) YSZ + $Fe_2O_3$.

Khigame and Yoshida's was that the Raman spectrum is mainly determined by the imperfect oxygen sublattice.

The Raman spectra of the present YSZ (spectrum A), YSZ/Cu (spectrum B) and YSZ/Fe (spectrum C) are shown in Fig. 5. The defect-induced Raman spectra show several low-frequency ( $< 600$ cm$^{-1}$) features apart from the $F_{2g}$ mode at around 600 cm$^{-1}$. The infrared reflectance spectra are broader, see Fig. 6, but reveal an overlap of several absorption modes below 600 cm$^{-1}$. The appearance of a peak/shoulder around 600 cm$^{-1}$ is indicative of the breakdown of the selection rule for centro-symmetric systems (assuming that it is the same vibration as the $F_{2g}$ mode in Raman and not a coincidental frequency overlap).

## 4. Discussion

The lower valent oxides such as CuO and $Fe_2O_3$ can dissolve in YSZ, as clearly indicated by our X-ray data.

The foreign metal ions should be smaller or comparable in size to the ionic radius of $Zr^{4+}$. This is clearly obeyed for $Cu^{2+}$ as well as $Fe^{3+}$. The ionic radii, according to Shannon [37] are: $r_{Cu(II)} = 0.073$ nm, $r_{Fe(III)} = 0.078$ nm and $r_{Zr(IV)} = 0.084$ nm (all for coordination number 8). The dopant ions can choose a zirconium ion site (substitutional doping) or an interstitial site. The two defect reactions are represented below in Kröger–Vink notation.

Substitutional doping (increase in number of unit cells)

$$CuO = Cu''_{Zr} + V_O.. + O^*_O \quad (5)$$

$$Fe_2O_3 = 2Fe'_{Zr} + V_O.. + 3O^*_O \quad (6)$$

Interstitial doping (constant number of unit cells)

$$CuO + V_O.. = Cu_i^{\cdot\cdot} + O^*_O \quad (7)$$

$$Fe_2O_3 + 3V_O.. = 2Fe_i^{\cdot\cdot\cdot} + 3O^*_O \quad (8)$$

The influence of doping via one mechanism or the other on the lattice parameter can be estimated as follows.

Substitutional model: the introduction of substitutional ions of small radii, as in Reactions 5 and 6, will probably have little effect on the lattice constant, which is largely determined by the larger oxygen ions. Reactions 5 and 6 indicate a (small) relative increase in vacancy concentration compared with undoped YSZ with the same yttria content. The lattice parameter versus mol % yttria relation determined by Ingel and Lewis [38] indicates expansion of the lattice with increasing vacancy concentration. The overall effect will be an expansion of the lattice. Because we are far beyond the maximum in conductivity in the $ZrO_2$–$Y_2O_3$ system, the ionic conductivity will decrease if the system chooses the substitutional doping scheme.

Interstitial model: the formation of interstitial ions, as in Reactions 7 and 8 will give rise to expansion of the lattice; however, the removal of oxygen vacancies will have the opposite effect. The conductivity argument predicts a higher conductivity if interstitial substitution takes place. If our observations and arguments are correct, we are thereby forced to assume that the substitutional doping takes place.

## Acknowledgement

One of the authors (F.W.P.) thanks the Council of the Nordic Ministers for a research grant, during which period the present work was completed.

## References

1. T. TAKAHASHI, Y. SUZUKI and T. YOSHIDA, *Denki Kagaku* **38** (1970) 51.
2. R. V. WILHELM Jr and D. S. HORWATH, *Ceram. Bull.* **58** (1979) 228.
3. M. J. VERKERK, A. J. A. WINNUBST and A. J. BURGGRAAF, *J. Mater. Sci.* **17** (1982) 3113.

4. N. MATSUI, *Solid State Ionics* **18/19** (1986) 888.
5. N. MATSUI and M. TAKIGAWA, *ibid.* **40/41** (1990) 926.
6. N. MATSUI, *Denki Kagaku* **59** (1991) 31.
7. S. DAVISON, R. KERSHAW, K. DWIGHT and A. WOLD, *J. Solid State Chem.* **73** (1988) 47.
8. P. BERTHET, J. BERTHON and A. REVCOLEVSCHI, *Phys. B* **158** (1989) 506.
9. H. P. BECK and C. KALIBA, *Mater. Res. Bull.* **25** (1990) 1161.
10. M. HARTMANOVÁ, L. MACHOVIC, A. KOLLER, F. HANIC and B. MISANIK, *Solid State Ionics* **14** (1984) 93.
11. M. JAYARATNA, M. YOSHIMURA and S. SOMIYA, *J. Mater. Sci.* **22** (1987) 2011.
12. P. J. ALONSO, R. ALCALA, J. CASAS-GONZALES, R. CASES and V. M. ORERA, *J. Phys. Chem. Solids* **50** (1989) 1185.
13. F. W. POULSEN, J. B. BILDE-SØRENSEN, K. GHANBARI-AHARI, G. G. KNAB and M. HARTMANOVÁ, *Solid State Ionics* **40/41** (1990) 947.
14. P. FABRY and M. KLEITZ, *J. Electrochem. Soc.* **126** (1979) 2183.
15. X.-M. LUO, P. WU, R. KERSHAW, K. DWIGHT and A. WOLD, *Mater. Res. Bull.* **23** (1988) 1719.
16. V. I. ALEKSANDROV, V. V. OSIKO, A. M. PROCHOROV and V.M. TATARINTSEV, *Uspechi Khimii* **47** (1978) 385.
17. E. D. CASE, J. R. SMYTH and V. MONTHEI, *J. Am. Ceram. Soc.* **64** (1981) C-24.
18. J. J. BENTZEN, N. H. ANDERSEN, F. W. POULSEN, O. T. SØRENSEN and R. SCHRAM, *Solid State Ionics* **28/30** (1988) 550.
19. J. E. BAUERLE, *J. Phys. Chem. Solids* **30** (1969) 2657.
20. M. V. INOZEMTSEV and M. V. PERFILEV, *Elektrokhim.* **11** (1975) 1031.
21. A. PAJARAS, F. GUIDBERTEAU, A. DOMINGUEZ-RODRIGUEZ and A. H. HEUER, *J. Am. Ceram. Soc.* **71** (1988) C-332.
22. G. N. MORSCHER, P. PIROUZ and A. H. HEUER, *ibid.* **74** (1991) 491.
23. F. HANIC, M. HARTMANOVÁ, A. A. URUSOVSKAYA, G. G. KNAB, N. A. IOFIS and I. L. ZYRYANOVA, *Solid State Ionics* **36** (1989) 197.
24. C. M. PHILIPI and K. S. MAZDIYASNI, *J. Am. Ceram. Soc.* **45** (1971) 254.
25. D. W. LIU, C. H. PERRY and R. P. INGEL, *J. Appl. Phys.* **64** (1988) 1415.
26. A. FEINBERG and C. H. PERRY, *J. Phys. Chem. Solids* **42** (1981) 513.
27. V. KERAMIDAS and W. WHITE, *J. Am. Ceram. Soc.* **67** (1984) 22.
28. M. ISHIGAME and T. SAKURAI, *ibid.* **60** (1977) 367.
29. C. H. PERRY, D. W. LIU and R. P. INGEL, *ibid.* **68** (1985) 184.
30. M. ISHIGAME and E. YOSHIDA, *Solid State Ionics* **23** (1987) 211.
31. B. PIRIU and H. ARASHI, *Bull. Mineral.* **103** (1980) 363.
32. D. W. LIU, C. H. PERRY, A. A. FEINBERG and R. CURRAT, *Phys. Rev. B* **36** (1987) 9212.
33. C.H. PERRY, F. LU, D.W. LIU and B. ALZYAB, *J. Raman Spectr.* **21** (1990) 577.
34. R. SHUKER and R. W. GAMMON, *Phys. Rev. Lett.* **25** (1970) 220.
35. R. LOUDON and W. HAYES, in "Scattering Light in Crystals" edited by W. Hayes and R. Loudon (Wiley, New York, 1978).
36. V. I. ALEKSANDROV, K. VORONKO, B. V. IGNATOV, E. E. LOMONOVA, V. V. OSIKO and A. A. SOBOL, *Solid State Phys.* **20** (1978) 321.
37. R. D. SHANNON, *Acta Crystallogr.* **A32** (1976) 751.
38. R. P. INGEL and D. LEWIS III, *J. Am. Ceram. Soc.* **69** (1986) 325.

*Received 26 January*
*and accepted 21 September 1993*